

# Ion kinetic-energy distributions in argon rf glow discharges

J. K. Olthoff and R. J. Van Brunt

National Institute of Standards and Technology,<sup>a)</sup> Gaithersburg, Maryland 20899

S. B. Radovanov

Institute of Physics, 11000 Belgrade, Yugoslavia

(Received 26 May 1992; accepted for publication 22 July 1992)

Kinetic-energy distributions have been measured for different mass-selected ions sampled from 13.56 MHz rf glow discharges in argon inside a "GEC rf reference cell." The electrode geometry of this cell produces an asymmetric discharge and the cell is operated in a pressure regime where ion-molecule collisions in the sheath region of the discharge are significant. Ions are sampled from the side of the plasma perpendicular to the interelectrode axis using an electrostatic energy analyzer coupled to a quadrupole mass spectrometer. Kinetic-energy distributions for  $\text{Ar}^+$ ,  $\text{Ar}_2^+$ ,  $\text{Ar}^{++}$ , and  $\text{ArH}^+$  are presented as functions of applied rf voltage, gas pressure, and distance of the mass spectrometer entrance aperture from the edge of the electrodes. The distributions obtained for the sampling orifice placed close enough to the electrodes to allow formation of a sheath in front of the orifice exhibit features similar to those observed previously when sampling ions through the grounded electrode of a parallel-plate reactor. The  $\text{Ar}^+$  and  $\text{Ar}^{++}$  distributions exhibit secondary maxima predicted to result from the formation of low-energy (thermal) ions in the sheath region, such as by charge-exchange and high-energy electron collisions. Kinetic-energy distributions for  $\text{Ar}_2^+$  and  $\text{ArH}^+$  exhibit no secondary maxima and are peaked at high energies indicative of the sheath potential, and consistent with a formation mechanism involving relatively low-energy collisions in the bulk plasma (glow region).

## I. INTRODUCTION

Ion bombardment plays a crucial role in anisotropic etching of semiconductor materials in rf plasmas.<sup>1</sup> It has been shown that etching anisotropy and rates are affected by variations in ion flux and ion kinetic energies.<sup>2-4</sup> For the production of future semiconductor devices it has been suggested that methods must be developed to ensure that bombarding ions exhibit narrow kinetic-energy distributions and that ion fluxes and mean energies are controllable.<sup>5</sup> The first step toward meeting these demands is to develop methods for monitoring bombarding ion currents, energies, and angular distributions, and to determine how these parameters vary with plasma conditions.

With these requirements in mind, a significant amount of experimental research has been performed to understand more fully the details of ion production in rf plasmas, and the interaction of ions with the plasma sheaths. A large portion of this work has been performed on argon plasmas because of the relative simplicity of the chemical and physical processes occurring in the plasma, and because of several industrial applications involving sputtering by argon ions. Coburn and Kay<sup>6</sup> performed some of the earliest investigations of ion kinetic-energy distributions in rf plasmas by utilizing an electrostatic kinetic-energy filter in conjunction with a quadrupole mass spectrometer to sample ions through an orifice in the grounded electrode. An extension of this technique was then used to determine plasma sheath potentials from measured  $\text{Ar}_2^+$  kinetic-

energy distributions,<sup>7</sup> and to determine the dependence of  $\text{ArH}^+$  and  $\text{Ar}_2^+$  kinetic energies on the frequency of the applied rf voltage.<sup>8</sup>

Green *et al.*<sup>9</sup> utilized a similar instrument in which the ion-energy filter was an on-axis cylindrical mirror analyzer (CMA).<sup>10</sup> Ion kinetic-energy distributions for  $\text{Ar}^+$  and  $\text{ArH}^+$  sampled from an rf argon discharge exhibited significant broadening effects with increasing gas pressure. The  $\text{Ar}^+$  kinetic-energy distributions also exhibited low-energy peaks whose positions and intensities varied with plasma conditions. Ingram and Braithwaite<sup>11</sup> utilized a retarding potential analyzer (RPA) with no mass analysis to observe similar broadening of ion kinetic-energy distributions from argon plasmas; however, no structure was observed in the distributions.

More recently, Wild and Koidl<sup>12</sup> also observed multiple peaks in ion kinetic-energy distributions sampled from an argon rf plasma. They attributed these peaks to correlations between the measured ion energy and the rf phase and position in the sheath at which thermal ions were formed by ion/neutral charge-exchange collisions. These conclusions were supported by Monte Carlo calculations that included charge-exchange interactions.<sup>12,13</sup> Liu, Huppert, and Sawin<sup>14</sup> reported similar observations of structure in the ion kinetic-energy distributions for argon plasmas using a modified RPA technique. Additionally, they measured energy distributions as a function of ion incident angle and determined that momentum-transfer scattering in the sheath is essential to produce ions with a significant velocity component parallel to the surface under bombardment. Toups and Ernie<sup>15</sup> also utilized a RPA to identify the ratio of the reactor gas pressure to the frequency of the

<sup>a)</sup>Electricity Division, Electronics and Electrical Engineering Laboratory, Technology Administration, U.S. Department of Commerce.

applied voltage as a critical parameter in characterizing the structure of the ion kinetic-energy distributions sampled from argon rf discharges.

Experiments have been performed to measure the kinetic-energy distributions of ions striking the powered electrode in rf reactors. Kuypers and Hopman<sup>16</sup> measured ion kinetic-energy distributions at the powered electrode of a cylindrical electrode discharge chamber by utilizing optical fibers to isolate the ion current signals from the rf voltage. Manenschijn *et al.*<sup>17</sup> performed a similar experiment in a parallel-plate discharge by using a low-pass filter for electrical isolation. Data from these experiments exhibited multiple peaks in qualitative agreement with experiments in which ions were sampled through the grounded electrode. May and co-workers<sup>13</sup> recently computed the trajectories of ions and neutrals through the sheath of an argon radio-frequency discharge using a Monte Carlo method. In their modeling they incorporate time-varying fields together with momentum-transfer and resonant charge-transfer collision processes. The calculated ion kinetic-energy distributions show structure in accordance with experimental data.

Most experimental investigations of ion kinetic-energy distributions in argon plasmas have not utilized mass analysis of the detected ion flux because of the increased experimental difficulties and because the ion current consists primarily of  $\text{Ar}^+$ . However, a detailed investigation of the energy distributions of the less-abundant ions in an argon discharge provides information concerning the formation of positive ions in the plasma, and about the interactions that affect ions in the sheath regions. Most previous investigations have also been concerned with ions that impinge on the electrode surfaces.

In this paper, we present measured kinetic-energy distributions for  $\text{Ar}^+$ ,  $\text{Ar}^{++}$ ,  $\text{Ar}_2^+$ , and  $\text{ArH}^+$  from a 13.56 MHz argon rf plasma over a wide range of rf voltages, gas pressures, and sampling positions in a configuration that has become known as the "GEC rf reference cell."<sup>18-21</sup> The ions were sampled along an axis midway between the parallel-plate electrodes and perpendicular to the interelectrode axis. The effects of sampling the ions from different positions relative to the discharge glow region are elucidated.

## II. EXPERIMENTAL APPARATUS

The GEC rf reference cell used for the present experiments has previously been described, and characterized by measurements performed in several different laboratories.<sup>18-21</sup> The cell is configured with 10.2-cm-diam aluminum electrodes with an interelectrode spacing of 2.54 cm. Argon gas (99.999% purity) was supplied to the plasma cell through a showerhead arrangement of small holes in the grounded upper electrode and pumped out through six symmetrically placed holes in the base of the reactor. The lower electrode was powered by a ENI 13.56 MHz rf power supply<sup>22</sup> coupled by a 0.1  $\mu\text{F}$  blocking capacitor. The plasmas were low power ( $< 2 \text{ W}$ ) with applied peak-to-peak voltages of 200 V, or less. Voltage and current wave forms and self-bias voltages were measured at the

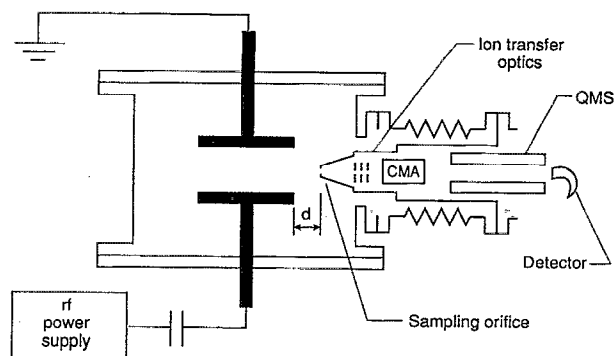


FIG. 1. Schematic diagram showing the orientation of the CMA-MS sampling cone with respect to the GEC reference cell electrode assembly. The distance  $d$  between the sampling orifice and the edge of the electrodes is variable from 0 to 10 cm. QMS is the quadrupole mass spectrometer.

powered electrode by a 300 MHz digital oscilloscope using a 200 MHz voltage probe and a 200 MHz Pearson coil.<sup>22</sup> The Fourier components of the wave forms were then derived by a fitting routine, and these values were used to calculate the current and voltage wave forms at the plasma.<sup>19</sup>

Ion kinetic-energy distributions were measured using a Vacuum Generators SXP300H<sup>22</sup> quadrupole mass spectrometer (MS) equipped with a CMA ion energy analyzer. The configuration is similar to that described by Krumme, Hack, and Raaijmakers.<sup>23</sup> The CMA-MS system was mounted to the GEC reference cell through a side port so that ions were sampled from the side of the plasma. A bellows assembly allowed the distance  $d$  between the sampling orifice and the edge of the electrodes to be varied from 0 to 10 cm. A schematic diagram showing the orientation of the CMA-MS relative to the electrode assembly is shown in Fig. 1. Although measurements were made using CMA-MS sampling cones with varying orifice sizes, all the data reported here were obtained using a 200- $\mu\text{m}$ -diam orifice in a grounded stainless-steel cone with a flattened end. Pressures in the analyzer did not exceed  $2 \times 10^{-4}$  Pa for plasma pressures up to 13.3 Pa due to differential pumping of the CMA-MS vacuum housing.

Even though ions were sampled from the side of the plasma (rather than through a grounded electrode), it is expected that as  $d \rightarrow 0$  the distributions will be similar to those that would be obtained when sampling through an electrode because a sheath is formed in front of the cone face. This will be discussed in more detail in the following section. The present geometry has the advantage of allowing ions to be sampled at various distances from the plasma region. This provides additional information related to sheath formation and ion-molecule interactions, and in many cases emulates a sampling arrangement that could be utilized on some commercial etching reactors.

A spectroscopic apparatus was used to investigate the effect of the position of the sampling cone on the uniformity of the optical emission from the plasma and to monitor plasma sheath locations. This apparatus has been described elsewhere.<sup>24</sup> Briefly, it consists of a  $\frac{2}{3}$  m Czerny-

Turner-type grating spectrometer equipped with a low-noise pulse-counting photomultiplier. The photon emission from the plasma is focused on the entrance slit of the monochromator by a series of mirrors. Horizontal profiles of the plasma may then be obtained by displacing the optical table and vertical scans of the emission profiles from the plasma by displacing the appropriate mirror.

### III. DATA ACQUISITION AND ANALYSIS

Ion kinetic-energy distributions were acquired by tuning the mass spectrometer to a particular mass-to-charge ratio and then scanning the energy of the ions entering the energy analyzer in such a way that the ions always pass through the CMA-MS with the same energy. An energy resolution of 0.5 eV (full width at half-maximum) was maintained over the entire energy range scanned. All data for a particular ion were obtained with the same integration time in order to allow comparison of relative ion intensities.

The raw data obtained with this instrument exhibit no ion signal for kinetic energies below approximately 3.5 eV.<sup>23,25</sup> Tests of the CMA-MS performance were made by connecting it to a uniform field drift tube in which  $K^+$  kinetic-energy distributions were measured in argon as a function of electric field-to-gas density ratio. These results clearly indicate an energy shift when compared with measurements made by others<sup>26</sup> under similar conditions. This energy shift was observed only when ions were sampled through the orifice in the cone, thus suggesting that charging occurs on the inner surfaces of the sampling cone in the low-pressure region of the CMA-MS which causes acceleration of ions from the orifice into the CMA. It might be expected that the outer surface of the cone, which is exposed to the plasma, would be less likely to hold a significant surface charge due to the constant bombardment of the surface by electrons and neutrals. Similar surface charging effects and energy shifts have been observed for other types of ion-energy analyzers.<sup>26</sup>

Taking into account the finite energy resolution of the CMA, a determination of the absolute kinetic-energy scale was made by arbitrarily assigning a value of 0 eV to the channel in which the  $Ar^+$  signal was first detected from an argon discharge. This is appropriate because the kinetic-energy distributions for  $Ar^+$  ions in argon discharges have been shown to extend down to 0 eV due to the production of very low-energy ions by resonant charge-exchange collisions.<sup>12-15</sup> The energy scales for all of the kinetic-energy distributions presented here have been adjusted to account for this energy shift. Based upon the estimated uncertainties in this technique and the resolution of the CMA, the uncertainty of the ion kinetic-energy scale is determined to be  $\pm 0.25$  eV.

Theoretical analysis of the effects of orifice size on ion sampling indicates that an orifice of comparable size to that used here may affect the trajectories, and therefore collection efficiencies, of ions with kinetic energies less than 5 eV.<sup>14,27</sup> Therefore the relative ion signal intensities can be expected to exhibit more uncertainty and become increasingly less representative of the true energy distribution as

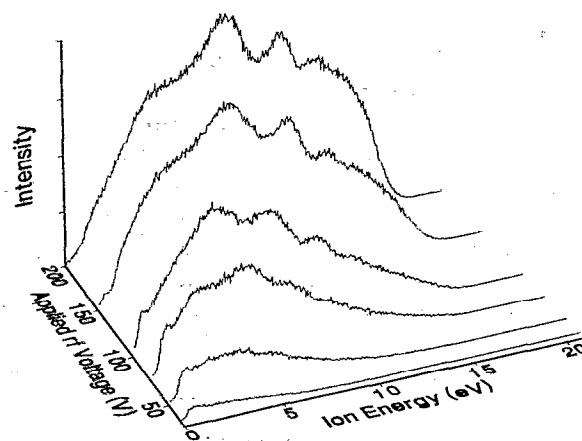


FIG. 2.  $Ar^+$  kinetic-energy distributions as a function of peak-to-peak voltage for a 13.3 Pa argon plasma with  $d=0$  cm.

the ion energy decreases below about 5 eV. Since most of the interesting structure in the distributions occurs above 5 eV, the low-energy discrimination effects at the orifice are not relevant to the interpretations of results presented here. Above 5 eV, the observed profiles of the kinetic-energy distributions exhibit a high degree of reproducibility.

### IV. RESULTS

#### A. $Ar^+$

Shown in Fig. 2 are the ion kinetic-energy distributions for  $Ar^+$  produced in an argon discharge as a function of applied peak-to-peak voltage  $V_{pp}$  for the probe positioned at the edge of the electrodes ( $d=0$  cm). At the highest voltages, the distributions exhibit a structure replete with secondary maxima. This structure consists of up to four secondary maxima and is somewhat similar to that observed previously in ion-energy distributions sampled through the grounded electrode of parallel plate reactors.<sup>12-15</sup> For the highest voltage ( $V_{pp}=200$  V), the maximum energy at which an ion signal was detected  $\epsilon_{max}$  is about 18.0 eV.

As the applied voltage decreases, the intensity of the  $Ar^+$  current decreases, and the mean energy shifts toward lower energies. The positions of the secondary maxima also shift toward lower energies, and the relative magnitude of the secondary structure diminishes as the applied voltage is reduced. The shift in mean energy is expected since reduction of the applied voltage decreases the magnitude of the electric field across the sheath and thus lowers the resulting ion energies.<sup>28</sup> For kinetic energies above 5 eV, the distributions are, as noted above, very reproducible, with intensities varying by less than 10% and with the positions of the secondary peaks varying by less than the estimated uncertainty of the energy scale. Below 5 eV, the intensities of the distributions fluctuated by as much as 30% from day to day. These variations may have been due, in part, to changes in the surface conditions of the cone containing

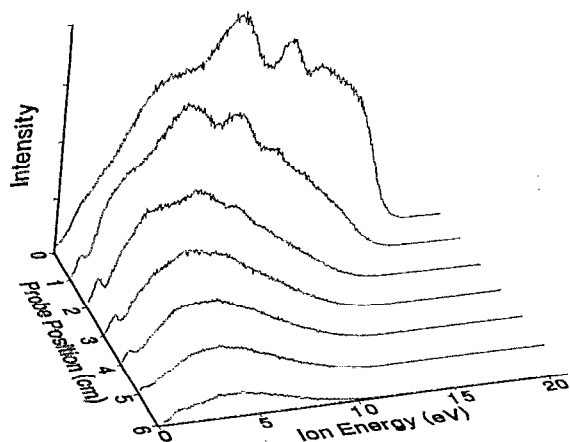


FIG. 3.  $\text{Ar}^+$  kinetic-energy distributions as a function of probe position for a 13.3 Pa argon plasma with  $V_{pp}=200$  V.

the orifice through which ions are sampled or, in part, to variations in plasma conditions which could not be controlled.

Figure 3 shows  $\text{Ar}^+$  kinetic-energy distributions as a function of the probe position  $d$  with respect to the edge of the electrodes. As  $d$  increases, the ion flux decreases, the energy distribution narrows, and the mean ion energy shifts to lower values. It is also seen that as the sampling cone is retracted from the electrodes, the secondary maxima begin to diminish in size and essentially disappear for  $d > 3.0$  cm. These trends are consistent with both a reduction in electric-field strength as  $d$  increases and a modification of the distribution resulting from the increased number of ion-molecule collisions in the path to the CMA-MS. The ion kinetic-energy distributions observed for the largest values of  $d$  are more indicative of the ion flux striking the walls of the vacuum chamber than that impinging on the electrode.

Figure 4 shows  $\text{Ar}^+$  kinetic-energy distributions as a function of gas pressure from 1.7 to 13.3 Pa. For pressures above 8 Pa, there is little observable change in the kinetic-energy distributions with decreasing pressure, except for a

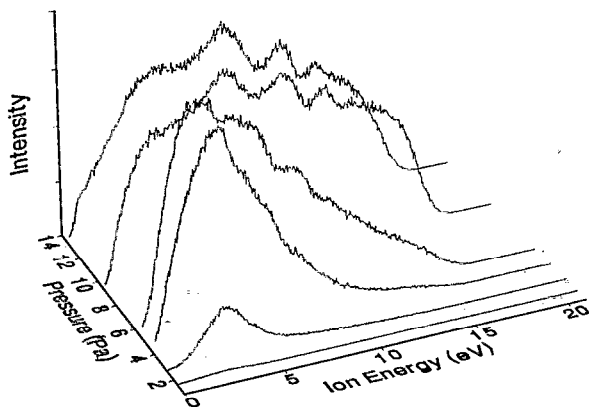


FIG. 4.  $\text{Ar}^+$  kinetic-energy distributions as a function of gas pressure for an argon plasma with  $d=0$  and  $V_{pp}=200$  V.

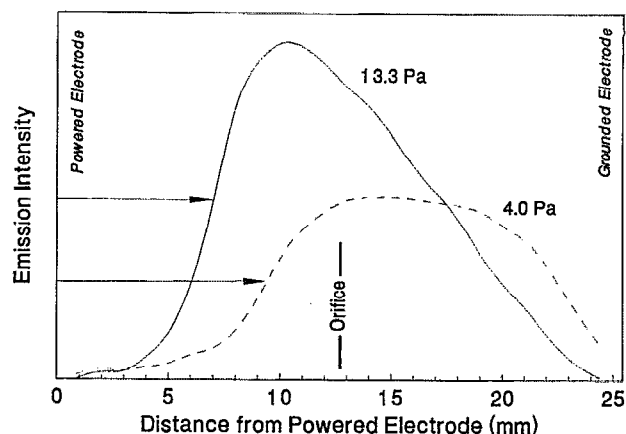


FIG. 5. Measured axial profile of Ar I 750.39 nm optical emission from a 200 V argon plasma at the indicated absolute gas pressures. The position of the ion sampling orifice is indicated, and the sheath widths in front of the powered electrode are indicated with arrows.

shift of the secondary maxima to lower energies similar to that observed by Wild and Koidl.<sup>12</sup> Below 8 Pa, the ion intensity drops and the distributions shift rapidly to lower energy with pressure. This latter effect is due to the fact that the sheath in front of the powered electrode expands in thickness as the pressure decreases. For gas pressures below about 6 Pa the sheath expands beyond the CMA-MS orifice and the sampling cone no longer plays an obvious role in defining the sheath, i.e., no actual sheath appears to exist between the cone face and the bulk plasma. This effect is illustrated by the comparison of the vertical optical emission profile data shown in Fig. 5 for argon plasmas with gas pressures of 13.3 and 4.0 Pa. At 13.3 Pa, the orifice is located near the center of the bulk plasma; however, at 4 Pa the location of the powered electrode sheath begins to approach the sampling orifice. As the pressure decreases further, the ions are sampled from the "dark region" of the plasma where the characteristics of ion transport to the orifice are expected to differ significantly from those that apply to the case where the bulk plasma exists in front of the cone.

## B. $\text{Ar}^{++}$

Peak count rates for  $\text{Ar}^{++}$  were approximately 12% of  $\text{Ar}^+$  peak count rates from a 200 V, 13.3 Pa argon plasma with  $d=0$ , as shown in Table I. This comparison of count rates for the different ions sampled from the plasma does not allow for possible mass discrimination effects of

TABLE I. Comparison of maximum peak ion count rates at  $V_{pp}=200$  V, argon pressure of 13.3 Pa, and  $d=0$  cm.

Ion	Peak count rates (counts/s)	Normalized count rates (ion/ $\text{Ar}^+$ )
$\text{Ar}^+$	28 000	1.00
$\text{Ar}^{++}$	3400	0.12
$\text{Ar}_2^+$	200	0.007
$\text{ArH}^+$	200	0.007

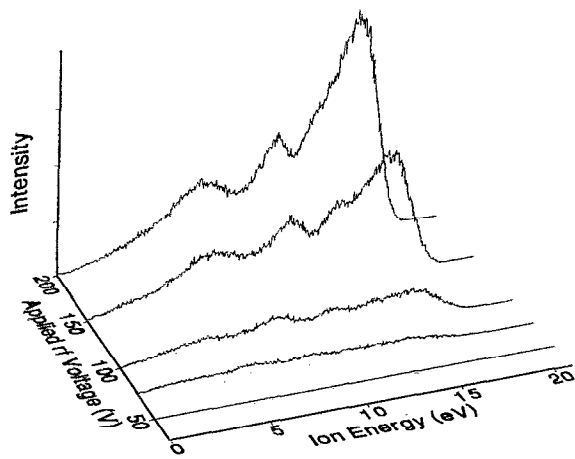


FIG. 6.  $\text{Ar}^{++}$  kinetic-energy distributions as a function of applied voltage for a 13.3 Pa argon plasma with  $d=0$ .

the quadrupole mass spectrometer system. However, it does indicate that a significant portion of the ion current in an argon plasma may consist of  $\text{Ar}^{++}$  and could possibly influence ion kinetic-energy distributions that do not employ mass selection.

Data for measured  $\text{Ar}^{++}$  kinetic-energy distributions are shown in Figs. 6–8. For conditions in which a sheath forms in front of the CMA-MS sampling cone, the  $\text{Ar}^{++}$  distributions tend to be peaked at the high-energy end and also exhibit secondary peaks. As in the case of  $\text{Ar}^+$ , up to four well-defined maxima can be distinguished in the distributions. The energy positions of these maxima are approximately the same as for  $\text{Ar}^+$ . The value of  $\epsilon_{\text{max}}$  at  $V_{\text{pp}}=200$  V is also the same as for  $\text{Ar}^+$ .

The dependencies on  $d$  and pressure are similar to those noted above for  $\text{Ar}^+$ . The intensity of the sampled  $\text{Ar}^{++}$  flux decreases rapidly as the sampling cone is withdrawn from the vicinity of the electrodes (Fig. 7). The secondary peaks in the distribution shift to lower energy as

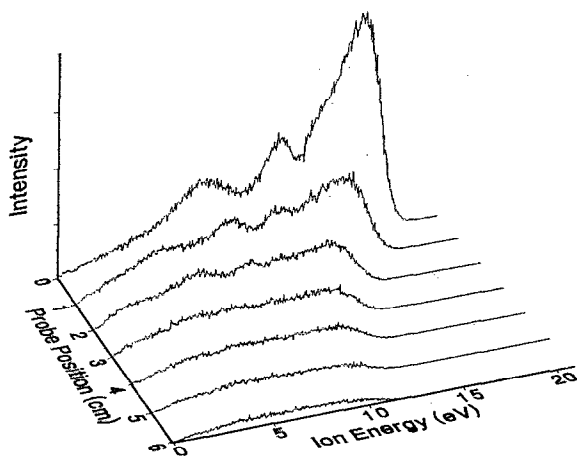


FIG. 7.  $\text{Ar}^{++}$  kinetic-energy distributions as a function of probe position for a 13.3 Pa argon plasma with  $V_{\text{pp}}=200$  V.

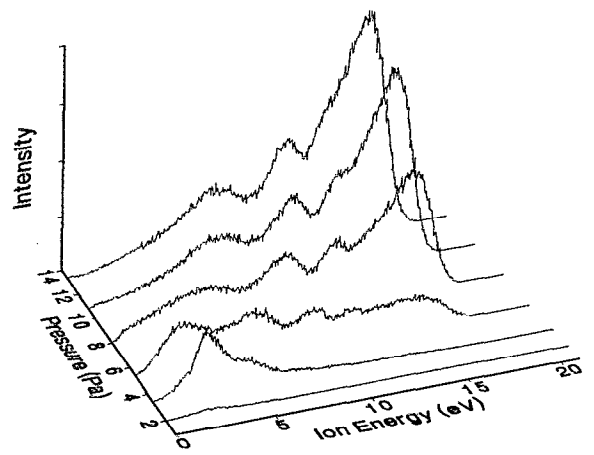


FIG. 8.  $\text{Ar}^{++}$  kinetic-energy distributions as a function of gas pressure for an argon plasma with  $V_{\text{pp}}=200$  V and  $d=0$ .

the pressure is reduced, and at pressures below about 3.5 Pa the distribution abruptly becomes peaked at the low-energy end because the sheath in front of the powered electrode expands beyond the level of the ion sampling aperture.

### C. $\text{Ar}_2^+$ and $\text{ArH}^+$

As seen in Table I, the intensities of  $\text{Ar}_2^+$  and  $\text{ArH}^+$  ions each constitute less than 1% of the detected ion signal under normal operating conditions. However, the  $\text{ArH}^+$  intensity was observed to vary with the amount of residual water present in the vacuum system, and larger  $\text{ArH}^+$  signals were observed when the cell was operated soon after the system was exposed to atmosphere.

Unlike  $\text{Ar}^+$  or  $\text{Ar}^{++}$ , the measured  $\text{Ar}_2^+$  and  $\text{ArH}^+$  kinetic-energy distributions shown in Figs. 9–12 lack secondary maxima. The  $\text{Ar}_2^+$  and  $\text{ArH}^+$  distributions are also narrower than those for  $\text{Ar}^+$  and  $\text{Ar}^{++}$  and are peaked at the high-energy end. The intensity of the  $\text{Ar}_2^+$  signal is not

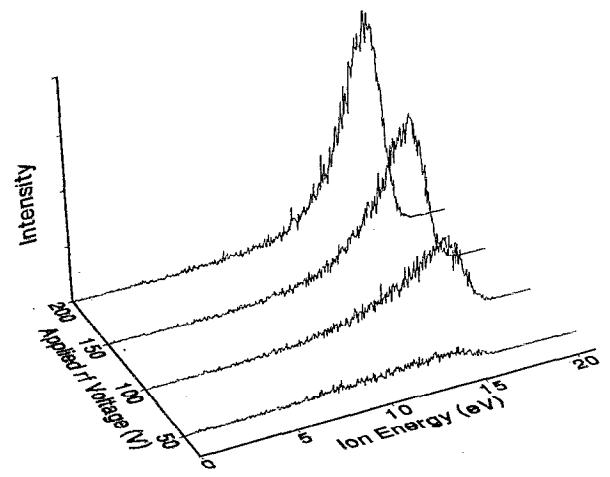


FIG. 9.  $\text{Ar}_2^+$  kinetic-energy distributions as a function of applied voltage for a 13.3 Pa argon plasma with  $d=0$ .

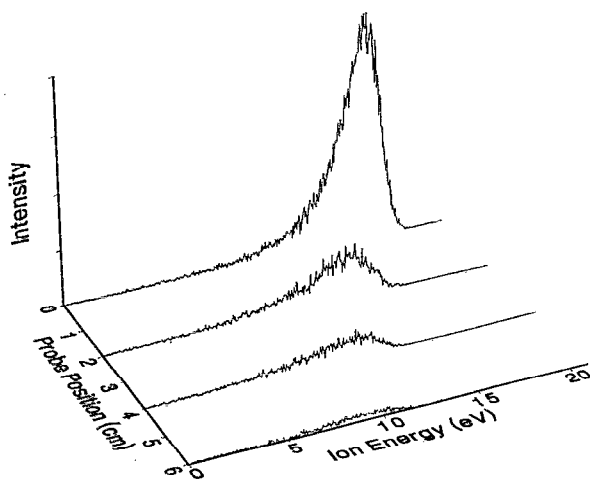


FIG. 10.  $\text{Ar}_2^+$  kinetic-energy distributions as a function of probe position for a 13.3 Pa argon plasma with  $V_{pp}=200$  V.

affected as dramatically by decreasing rf voltage as observed for  $\text{Ar}^{++}$  in Fig. 6, nor is the shape of the distribution modified as significantly as observed for  $\text{Ar}^+$  in Fig. 2. The dependence of the  $\text{Ar}_2^+$  kinetic-energy distributions for  $\text{Ar}_2^+$  on probe position and pressure are shown in Figs. 10 and 11, respectively. As  $d$  increases, the intensity and mean energy decrease due to the increased number of collisions experienced by ions before they are extracted into the analyzer. As the pressure decreases, the distributions again show little change until the pressure drops below 6.7 Pa.

Figure 12 shows several kinetic-energy distributions for  $\text{ArH}^+$  observed at different gas pressures. The detected ion intensities are substantially smaller than those observed for  $\text{Ar}^+$  and  $\text{Ar}^{++}$ . The characteristics of the  $\text{ArH}^+$  energy distributions are seen to be similar to those for  $\text{Ar}_2^+$ . The  $\epsilon_{\text{max}}$  values for both  $\text{Ar}_2^+$  and  $\text{ArH}^+$  are the same as for  $\text{Ar}^+$  and  $\text{Ar}^{++}$ .

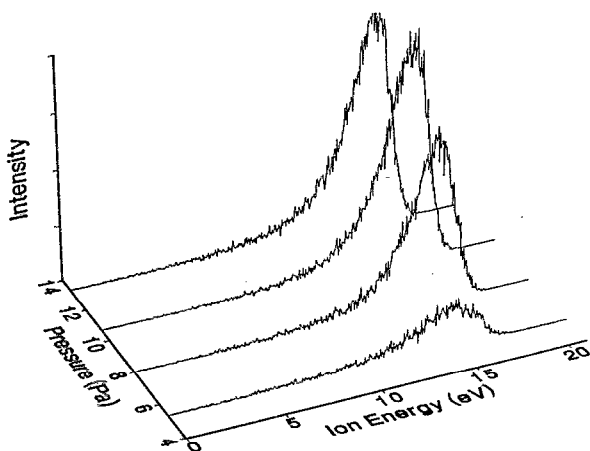


FIG. 11.  $\text{Ar}_2^+$  kinetic-energy distributions as a function of gas pressure for an argon plasma with  $d=0$  and  $V_{pp}=200$  V.

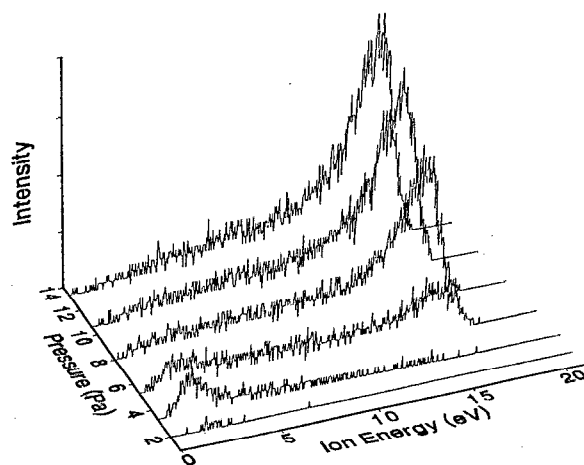


FIG. 12.  $\text{ArH}^+$  kinetic-energy distributions as a function of gas pressure for an argon plasma with  $V_{pp}=200$  V and  $d=0$ .

#### D. Influence of ion sampling probe on the plasma

It is of interest to consider the effect that the ion sampling probe has on the uniformity of the plasma. This is of practical concern in assessing the perturbing influences that result from sampling of ions at a side location perpendicular to the interelectrode axis. To investigate these effects, a detailed analysis of the rf voltage and current wave forms as a function of probe position was performed. The voltage and current wave forms were measured at the base of the powered electrode and then analyzed to determine the first three Fourier components of the waveforms. The results are presented in Table II where  $I_i$  is the amplitude of the  $i$ th harmonic of the current measured near the powered electrode,  $V_i$  is the amplitude of the  $i$ th harmonic for the voltage measured near the powered electrode,  $\phi_i$  is the phase of  $V_i$  relative to  $I_b$  and  $V_b$  is the self-bias potential. It should be noted that  $i=1$  refers to the fundamental component of the wave forms at 13.56 MHz. The data in Table II indicate no clear dependence of the currents, voltages, or phases on the probe position.

An investigation of the horizontal optical emission profile for the Ar 415.86 nm line as a function of probe position also indicated no measurable change in emission intensity at pressures near 13 Pa. At higher gas pressures, however, the optical emission profile is affected by the proximity of the probe to the electrodes. Figure 13 shows an optical emission profile taken at the midplane between the electrodes for argon pressures of 13 and 84 Pa. For 13 Pa the differences between the two scans is less than the random fluctuations in the emission intensity. Near +50 mm the probe intercepts the viewing range of the spectrometer, causing a decrease in the detected emission intensity. For 84 Pa, the horizontal spatial dependence of the emission intensity of this transition is somewhat modified as the mass spectrometer probe position is varied, thus indicating an influence on the plasma. However, at the pressures used for the experiments presented here ( $< 14$  Pa) the plasma is surprisingly unaffected by the presence of the sampling cone.

TABLE II. Amplitudes of the first three harmonics of the current and voltage wave forms measured near the powered electrode, their relative phases, and self-bias potentials  $V_b$  as a function of the sampling probe position  $d$  for a 200 V, 13.3 Pa argon plasma. These values are "raw" data as measured by the oscilloscope, and do not represent the voltage and current wave forms across the plasma. Thus these values may not be compared directly with standard GEC rf reference cell data presented elsewhere (Ref. 19).

$d$ (cm)	Current (mA)			Voltage (V)				Phase (deg)		
	$I_1$	$I_2$	$I_3$	$V_1$	$V_2$	$V_3$	$V_b$	$\phi_1$	$\phi_2$	$\phi_3$
0	225	46	212	96.7	1.8	0.5	-83.5	-63.6	105.2	-153.7
2	221	46	209	96.1	1.6	0.6	-83.2	-63.4	105.5	-163.0
4	220	46	210	96.8	1.7	0.6	-83.9	-64.3	107.2	-165.1
6	221	47	213	97.9	1.5	0.5	-85.5	-65.5	109.7	-149.9

## V. DISCUSSION

The ion kinetic-energy distributions observed here for the different ions produced by a 13.56 MHz rf discharge in argon can be interpreted in terms of the expected influence that the grounded ion sampling probe has in defining the sheath region of the discharge. When a sheath develops in front of the probe, the observed ion kinetics should be similar to those that apply to observations made through the grounded electrode. The sampling orifice cone can be considered in this case to behave as an extension of the grounded electrode.<sup>29</sup>

The observed structure (secondary maxima) in the  $\text{Ar}^+$  energy distributions can be attributed to phase-modulation effects associated with formation of low-energy

(thermal)  $\text{Ar}^+$  ions predominantly by resonant charge-transfer collisions in the sheath.<sup>12</sup> Similar secondary maxima in the  $\text{Ar}^{++}$  kinetic-energy distributions are presumably due to formation of these ions in the sheath by high-energy, electron-neutral collisions. In both cases the structure is predicted<sup>13</sup> to be broadened due to the effect of momentum transfer by elastic ion-molecule collisions.

The relatively broad kinetic-energy distributions seen for  $\text{Ar}^+$  have maxima at energies considerably below  $\epsilon_{\text{max}}$  suggesting that the detected ions are predominately formed in the sheath region. The  $\text{Ar}^+$  ions that are initially formed in the bulk of the plasma by electron impact can only account for a relatively small fraction of the observed distribution. Unlike the  $\text{Ar}^+$  distributions, the  $\text{Ar}^{++}$  distributions seen in Fig. 6 are peaked at the high-energy end (near  $\epsilon_{\text{max}}$ ) thus suggesting that the detected  $\text{Ar}^{++}$  ions are formed with the highest probability near the sheath-plasma boundary. The  $\text{Ar}^{++}$  intensity also shows a more rapid drop off with decreasing  $V_{\text{pp}}$  than is the case for the  $\text{Ar}^+$  intensity.

The tendency for the  $\text{Ar}_2^+$  to be peaked at the high-energy end is consistent with the expectation that these ions are formed by low-energy, three-body collisions in the low-field regions within the bulk of the plasma.<sup>30,31</sup> The  $\text{Ar}_2^+$  ions experience some energy loss by collisions as they travel through the sheath region, as is evident by the low-energy tails in the measured distributions. It is also possible that some  $\text{Ar}_2^+$  ions are lost by processes such as dissociative charge transfer. The relevant cross sections for  $\text{Ar}_2^+ + \text{Ar}$  collisions are not yet well determined.<sup>32</sup> The distributions in Fig. 9 are consistent with previous ion-energy measurements for  $\text{Ar}_2^+$  obtained by Köhler *et al.*<sup>7</sup> using a spherical energy analyzer sampling through a grounded electrode.

The fact that the  $\text{ArH}^+$  energy distributions are peaked at the high-energy end suggests that these ions are also formed by low-energy collisions in the bulk of the plasma. The mechanism for  $\text{ArH}^+$  formation is not known, but appears to depend upon the presence of water vapor as a gas impurity. This is supported by qualitative correlations between the measured  $\text{ArH}^+$  and  $\text{H}_2\text{O}^+$  ion intensities in the argon plasmas. As in the case of  $\text{Ar}_2^+$ , the long low-energy tails in the  $\text{ArH}^+$  distributions extending down to near 0 eV indicate that a substantial fraction of these ions experience energy loss by collisions in the sheath.

It was noted that for a given peak voltage and gas pressure, all ions have approximately the same maximum kinetic energy. For the type of rf discharge considered in the present experiment, the observed ions obtain most of their energy by traversing the sheath potential as they are accelerated from the bulk plasma toward a surface. In traversing the sheath, ion kinetic energies are reduced by ion-neutral collisions that result in momentum and energy transfer as noted above.

For 13.56 MHz argon plasmas, the maximum kinetic energy acquired by an ion as it travels across the sheath from the bulk plasma to the surface is indicative of the average plasma potential because the transit time is much

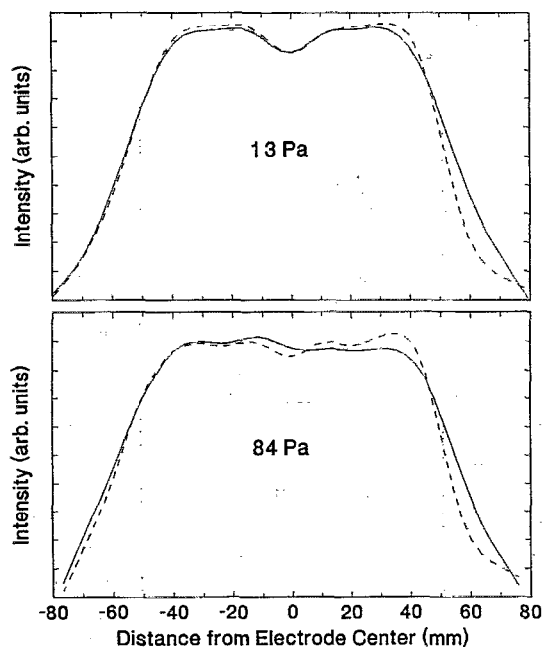


FIG. 13. Effect of the mass spectrometer probe on the optical emission spatial profile (at 415.86 nm) with the probe extended (---) and retracted (—) for 13 and 84 Pa argon plasmas with  $V_{\text{pp}}=200$  V. The vertical dotted line indicates the location of the electrode edges and the ion sampling probe is positioned on the right-hand side of the plasma.

greater than a single rf cycle. For plasmas with sheaths that are mostly capacitive, such as is the case for argon, it has been suggested<sup>7</sup> that the maximum kinetic energy of ions crossing a sheath may be approximated by

$$\epsilon_{\max} \approx (V_{\text{pl}} - |V_b|)/2, \quad (1)$$

where  $V_{\text{pl}}$  is the calculated voltage at the surface of the powered electrode,<sup>19,21</sup> and  $V_b$  is the self-bias potential where  $V_{\text{pl}} > |V_b|$ . In general, the maximum ion energies should lie within the range

$$V_{\text{pl}} - |V_b| > \epsilon_{\max} > (V_{\text{pl}} - |V_b|)/2.$$

In all cases, the observed maxima fall within this range. For example, at a peak voltage and gas pressure, respectively, of 200 V and 13.3 Pa, the sum of the bias potential and  $V_{\text{pl}}$  is approximately 27 eV and the measured value of  $\epsilon_{\max}$  is approximately 18.5 eV for  $\text{Ar}^+$  (see Fig. 2). The fact that the observed maximum is greater than predicted by Eq. (1) is to be expected since this formula does not take into account the floating potential or resistive component of the plasma. The off-axis sampling geometry may also affect the validity of Eq. (1) for this experiment.

It should be noted that the maximum kinetic energies observed here are significantly lower than those reported by Liu and co-workers<sup>14</sup> and Touns and Ernie<sup>15</sup> for similar argon plasmas. This is because the bias potentials  $V_b$  in their rf systems are less negative due to the confinement of the plasmas inside insulating cylinders. Confinement of the plasma equalizes the effective areas of the electrodes, thus reducing the magnitude of the self-bias potential with a resulting increase in the voltage drop across the sheath in front of the grounded electrode.

It was observed here for all ions that as the ion sampling probe is removed from the plasma region, so that there is no longer a well-defined sheath in the immediate vicinity of the probe, there is a loss of ion intensity and reduction in mean energy. Structure in the ion kinetic-energy distributions also disappears rapidly with increasing sampling distance. These trends are consistent with the expected randomizing effects associated with a corresponding increase in the number of collisions that can occur with increasing distance before the ions are analyzed, and with the reduction of the electric-field strength in the region in front of the sampling cone.

## VI. CONCLUSIONS

Kinetic-energy distributions have been measured for  $\text{Ar}^+$ ,  $\text{Ar}^{++}$ ,  $\text{Ar}_2^+$ , and  $\text{ArH}^+$  ions sampled from an argon parallel-plate rf discharge. The experimental geometry used allowed the sampling of ions from the side of the discharge, rather than through an electrode. The measured ion kinetic-energy distributions obtained using this sampling orientation, under conditions where the ion sampling element can be treated as effectively being part of the grounded electrode, exhibit features similar to those expected when sampling through the grounded electrode. Under conditions where the sampling element is removed from the plasma region it is found that observed ion inten-

sities and mean energies rapidly decrease due to intervening collisions of ions with the gas and reduced electric-field strength. No significant changes in the plasma were observed due to the proximity of the probe to the plasma.

Comparison of the kinetic-energy distributions for the different ions sampled from an argon discharge showed that each distribution was indicative of the origin of the ion and the interactions experienced as the ion crossed the sheath region into the sampling orifice. The kinetic-energy distributions for  $\text{Ar}^+$  and  $\text{Ar}^{++}$  exhibit structure due to formation of these ions in the sheath respectively by resonant charge-transfer collisions and electron-impact ionization. Because the ions experience significant collisional interactions in the sheath, the observed kinetic-energy distributions are strongly affected by changes in the sheath characteristics caused by changes in the pressure and voltage. Kinetic-energy distributions for  $\text{Ar}_2^+$  and  $\text{ArH}^+$  are nearly featureless because these ions appear to be created predominantly in the bulk of the plasma by low-energy collision processes. The formation of  $\text{ArH}^+$  appears to be correlated with the presence of water vapor.

## ACKNOWLEDGMENTS

This work was funded in part by SEMATECH, Austin, Texas. The authors would like to thank J. R. Roberts and S. Djurović for providing the optical emission data, M. A. Sobolewski and J. R. Whetstone for help with the voltage and current wave form measurements, and J. A. Rees for helpful discussions.

- <sup>1</sup>B. Chapman, *Glow Discharge Processes* (Wiley, New York, 1980).
- <sup>2</sup>J. W. Coburn and H. F. Winters, *J. Vac. Sci. Technol.* **16**, 391 (1979).
- <sup>3</sup>H. F. Winters, J. W. Coburn, and T. J. Chuang, *J. Vac. Sci. Technol. B* **1**, 469 (1983).
- <sup>4</sup>J. W. Coburn and H. F. Winters, *J. Appl. Phys.* **50**, 3189 (1979).
- <sup>5</sup>J. M. Cook and K. G. Donohoe, *Solid State Technol.* **34**, 119 (1991).
- <sup>6</sup>J. W. Coburn and E. Kay, *J. Appl. Phys.* **43**, 4965 (1972).
- <sup>7</sup>K. Köhler, J. W. Coburn, D. E. Horne, E. Kay, and J. H. Keller, *J. Appl. Phys.* **57**, 59 (1985).
- <sup>8</sup>K. Köhler, D. E. Horne, and J. W. Coburn, *J. Appl. Phys.* **58**, 3350 (1985).
- <sup>9</sup>W. M. Greene, M. A. Hartney, W. G. Oldham, and D. W. Hess, *J. Appl. Phys.* **63**, 1367 (1988).
- <sup>10</sup>H. Z. Sar-el, *Rev. Sci. Instrum.* **38**, 1210 (1967).
- <sup>11</sup>S. G. Ingram and N. St. J. Braithwaite, *J. Phys. D* **21**, 1496 (1988).
- <sup>12</sup>Ch. Wild and P. Koidl, *Appl. Phys. Lett.* **54**, 505 (1989); *J. Appl. Phys.* **69**, 2909 (1991).
- <sup>13</sup>P. W. May, D. Field, and D. F. Klemperer, *J. Appl. Phys.* **71**, 3721 (1992).
- <sup>14</sup>J. Liu, G. L. Huppert, and H. H. Sawin, *J. Appl. Phys.* **68**, 3916 (1990).
- <sup>15</sup>M. F. Touns and D. W. Ernie, *J. Appl. Phys.* **68**, 6125 (1990).
- <sup>16</sup>A. D. Kuypers and H. J. Hopman, *J. Appl. Phys.* **67**, 1229 (1990).
- <sup>17</sup>A. Manenschijn, G. C. A. M. Janssen, E. von der Drift, and S. Radelaar, *J. Appl. Phys.* **69**, 1253 (1991).
- <sup>18</sup>J. R. Roberts, J. K. Olthoff, R. J. Van Brunt, and J. R. Whetstone, *Advanced Techniques for Integrated Circuit Processing* (Society of Photo-Optical Instrumentation Engineers, Bellingham, WA, 1991), Vol. 1392, pp. 428-436.
- <sup>19</sup>P. J. Hargis, K. E. Greenberg, P. A. Miller, J. B. Gerardo, J. R. Torcynski, M. E. Riley, G. A. Hebner, J. R. Roberts, J. K. Olthoff, J. R. Whetstone, R. J. Van Brunt, M. A. Sobolewski, H. M. Anderson, M. Splichal, J. L. Mock, P. Bletzinger, A. Garscadden, R. A. Gottscho, G. Selwyn, M. Dalvie, J. E. Heidenreich, J. W. Butterbaugh, M. L. Brake, M. L. Passow, J. Pender, A. Lujan, M. E. Elta, D. B. Graves, H. H. Sawin, M. J. Kushner, J. T. Verdeyen, R. Horwath, and T. R. Turner, *Rev. Sci. Instrum.* (in press). This paper describes the design of the

- GEC rf reference cell, and presents a simple model for determination of the voltage and current wave forms at the powered electrode.
- <sup>20</sup>P. A. Miller, H. Anderson, and M. P. Spichal, *J. Appl. Phys.* **71**, 1171 (1992).
- <sup>21</sup>M. A. Sobolewski, *J. Vac. Sci. Technol. A* (in press). This paper describes a more accurate method for the determination of the current and voltage wave forms at the surface of the powered electrode in the GEC rf reference cell.
- <sup>22</sup>The identification of commercial materials and their sources is made to describe the experiment adequately. In no case does this identification imply recommendation by the National Institute of Standards and Technology, nor does it imply that the instrument is the best available.
- <sup>23</sup>J. P. Krumme, R. A. A. Hack, and I. J. M. M. Raaijmakers, *J. Appl. Phys.* **70**, 6743 (1991).
- <sup>24</sup>J. K. Olthoff, J. R. Roberts, R. J. Van Brunt, J. R. Whetstone, M. A. Sobolewski, and S. Djurovic, *Process Module Metrology, Control, and Clustering* (Society for Photo-Optical Instrumentation Engineers, Bellingham, WA, 1992), Vol. 1594, pp. 168–178.
- <sup>25</sup>S. B. Radovanov, J. K. Olthoff, and R. J. Van Brunt, in Proceedings of the International Conference on Phenomena in Ionized Gases, edited by V. Palleski and M. Vaselli, 1991 pp. 835–836. An equipment malfunction caused the ion-energy distributions presented in this paper to be in error; however, the conclusions drawn are still valid.
- <sup>26</sup>T. Makabe and H. Shinada, *J. Phys. D* **18**, 2385 (1985).
- <sup>27</sup>B. E. Thompson, K. D. Allen, A. D. Richards, and H. H. Sawin, *J. Appl. Phys.* **59**, 1890 (1986).
- <sup>28</sup>T. Makabe, N. Nakamo, and Y. Yamaguchi, *Phys. Rev. A* **45**, 2520 (1992).
- <sup>29</sup>Preliminary experimental results indicate that kinetic-energy distributions of ions sampled through the grounded electrode of a GEC rf reference cell do not differ significantly from those presented in this paper [J. A. Rees (unpublished)].
- <sup>30</sup>R. Johnsen, A. Chen, and M. A. Biondi, *J. Chem. Phys.* **73**, 1717 (1980).
- <sup>31</sup>M. Grossl, M. Langeirwalter, H. Helm, and T. D. Mark, *J. Chem. Phys.* **74**, 1728 (1981).
- <sup>32</sup>A. V. Phelps, *J. Phys. Chem. Ref. Data* **20**, 557 (1991).